IOP Publishing Journal of Physics B: Atomic, Molecular and Optical Physics
J. Phys. B: At. Mol. Opt. Phys. **47** (2014) 115302 (11pp) doi:10.1088/0953-4075/47/11/115302

Zero-momentum coupling induced transitions of ground states in Rashba spin–orbit coupled Bose–Einstein condensates

Jingjing Jin[1], **Suying Zhang**[1] **and Wei Han**[2]

[1] Institute of Theoretical Physics, Shanxi University, Taiyuan 030006, People's Republic of China
[2] Beijing National Laboratory for Condensed Matter Physics, Institute of Physics, Chinese Academy of Sciences, Beijing 100190, People's Republic of China

E-mail: zhangsy@sxu.edu.cn

Received 11 November 2013, revised 3 April 2014
Accepted for publication 16 April 2014
Published 13 May 2014

Abstract

We investigate the transitions of ground states induced by zero momentum (ZM) coupling in pseudospin-1/2 Rashba spin–orbit coupled Bose–Einstein condensates confined in a harmonic trap. In a weak harmonic trap, the condensate presents a plane wave (PW) state, a stripe state or a spin polarized ZM state, and the particle distribution of the stripe state is weighted equally at two points in the momentum space without ZM coupling. The presence of ZM coupling induces an imbalanced particle distribution in the momentum space, and leads to the decrease of the amplitude of the stripe state. When its strength exceeds a critical value, the system experiences the transition from stripe phase to PW phase. The boundary of these two phases is shifted and a new phase diagram spanned by the ZM coupling and the interatomic interactions is obtained. The presence of ZM coupling can also achieve the transition from ZM phase to PW phase. In a strong harmonic trap, the condensate exhibits a vortex lattice state without ZM coupling. For the positive effective Rabi frequency of ZM coupling, the condensate is driven from a vortex lattice state to a vortex-free lattice state and finally to a PW state with the increase of coupling strength. In addition, for the negative effective Rabi frequency, the condensate is driven from a vortex lattice state to a stripe state, and finally to a PW state. The stripe state found in the strong harmonic trap is different from that in previous works because of its nonzero superfluid velocity along the stripes. We also discuss the influences of the ZM coupling on the spin textures, and indicate that the spin textures are squeezed transversely by the ZM coupling.

Keywords: Bose–Einstein condensates, spin–orbit coupling, zero momentum coupling, transitions of groud states

(Some figures may appear in colour only in the online journal)

1. Introduction

The realization of the spin–orbit (SO) coupling in Bose–Einstein condensates (BECs) [1] provides us opportunities to study the SO effects in ultracold atoms. It also provides us an experimental platform to simulate and study the SO effects in condensed-matter systems by manipulating cold atoms, as the SO coupling is crucial for spin Hall effects [2, 3], spintronics [4, 5] and topological insulators [6–8]. The SO coupling in BECs has attracted the attention of a great deal of researchers because almost all parameters of the system can be controlled. Under the competition among the SO coupling, the interatomic interactions, the external potential and the rotation, some novel ground-state phases have been predicted, such as

plane wave (PW) phases, stripe phases, vortex lattice (VL) phases, and giant vortex [9–23]. These nontrivial phases have greatly enriched the ground state phases of the BEC system.

As we known, multi-component BECs confined in a single well with a coherent coupling can be realized in experiments by performing an external driving field [24, 25], and will give rise to many interesting phenomenons, such as immiscibility–miscibility transition, formation of vortex molecules, internal Josephson junctions and so on [26–30]. In addition, there has been a large experimental progress about BECs in the synthetic effective magnetic fields that combined Raman coupling with radiofrequency coupling [31]. In the previous works about SO coupled BECs, Wang *et al* concluded that with a weak harmonic trap, the condensate presents the PW phase ($g > g_{12}$) or stripe phase ($g < g_{12}$), depending on the competition between the intra- and inter-component interactions [9]. Furthermore, Yu indicated that in addition to these two phases, there exists another phase, namely a spin polarized zero momentum (ZM) phase [32]. For the condensate with a strong harmonic trap, the VL phases were theoretically predicted by Hu *et al* [17]. These works, however, consider just only one kind of coupling on BECs. We are inspired to research whether there will exist novel structures or new phenomenons when we consider adding another coupling which named ZM coupling contrasting to Raman coupling to SO coupled systems.

The aim of this paper is to study the effect of ZM coupling on pseudospin-1/2 Rashba SO coupled BECs confined in a harmonic trap. Firstly, we consider the condensate with a weak harmonic trap. The ZM coupling induces an imbalanced particle distribution of the stripe state in k-space, and this imbalance leads to the amplitude of spin density stripe decrease. So we can realize the adjusting of the stripe's amplitude by performing a ZM coupling on the system. When the strength of ZM coupling exceeds a critical value, the condensate experiences the transition from a stripe phase to a PW phase. The phase boundary between the stripe phase and the PW phase is shifted and the scope of parameters of the PW phases is expanded. In addition, the ZM coupling can also achieve the transition from spin polarized ZM phase to PW phase.

We also study the condensate with a strong harmonic trap. In the absence of ZM coupling, vortices appear in pairs in each component forming a honeycomb vortex–antivortex (VA) lattice, and their arrangement leads to three kinds of spin textures: ±half-quantum vortices (HQV) and spin-2 texture. We turn on the ZM coupling from the vortex state, and respectively discuss the impacts of the positive and negative effective Rabi frequency on the structures of the ground states. For the positive effective Rabi frequency, the vortex and antivortex in each component are close to and finally annihilate each other with the increasing of ZM-coupling strength, forming a vortex-free lattice (VFL) state. With the further increase of ZM coupling, the condensate becomes the PW state finally. We also investigate the pseudospin textures and find that the spin density vectors pointing to the x direction are restrained, and the spin density vectors cover the Bloch sphere from a complete sphere to an incomplete one and finally to a point with the increase of ZM coupling. For the negative effective Rabi frequency, the condensate experiences the transition from a VL state to a stripe state. This stripe state is different from that in previous works because of its nonzero superfluid velocity along the stripes. As ZM coupling increases further, the condensate becomes the PW state finally.

This paper is organized as follows: in section 2, we introduce the model Hamiltonian and investigate the single-particle ground state of the system. In section 3, we investigate the mean-field ground states of the SO and ZM coupled BECs. With a weak and strong harmonic trap, the transitions of the ground states driven by ZM coupling are numerically studied, respectively. The experimental proposal is discussed in section 4, and the conclusions are given in section 5.

2. Model Hamiltonian and single-particle ground state

We consider a pseudospin 1/2 BEC in a quasi-2D harmonic trap $V = \frac{1}{2}m\left[\omega_\perp^2(x^2+y^2)+\omega_z^2 z^2\right]$ with Rashba SO and ZM coupling, where $\omega_z/\omega_\perp = \eta \gg 1$. The model Hamiltonian can be given by $\mathcal{H} = \mathcal{H}_0 + \mathcal{H}_{\rm int}$,

$$\mathcal{H}_0 = \int \mathrm{d}\mathbf{r}\Psi^\dagger\left[\frac{\hbar^2\mathbf{k}^2}{2m} + V + \kappa\hbar\mathbf{k}\cdot\vec{\sigma} + \lambda\sigma_x\hbar\right]\Psi, \tag{1a}$$

$$\mathcal{H}_{\rm int} = \int \mathrm{d}\mathbf{r}\left[\frac{g_{11}}{2}|\psi_1|^4 + \frac{g_{22}}{2}|\psi_2|^4 + g_{12}|\psi_1|^2|\psi_2|^2\right], \tag{1b}$$

where $\Psi = [\psi_1, \psi_2]^T$ is normalized as $\sum_j \int |\psi_j|^2 \ \mathrm{d}\mathbf{r} = N$, and N is the total number of particles in two components. $\mathbf{k} = \{k_x, k_y\}$ denotes xy-PW vectors, and $\vec{\sigma} = \{\sigma_x, \sigma_y\}$ are the 2×2 Pauli matrices. κ denotes the strength of SO coupling, and λ is the effective Rabi frequency to denote the strength of ZM coupling. $g_{jk} = 4\pi\hbar^2 a_{jk}/m$, $(j,k = 1,2)$ represents the intra-(g_{11}, g_{22}) or inter-component (g_{12}) interaction strength characterized by the s-wave scattering length a_{jk} and particle mass m.

In the absence of trap, the single-particle Hamiltonian presents two eigenenergy branches

$$E_\pm = \frac{\hbar^2\mathbf{k}^2}{2m} \pm \sqrt{(\kappa\hbar k_x + \lambda\hbar)^2 + (\kappa\hbar k_y)^2}, \tag{2}$$

with SO and ZM coupling. The single-particle ground state energy is in the E_- branch. We know that if we only consider the SO coupling in our system, i.e. $\lambda = 0$, the single-particle ground state is infinitely degenerate and characterized by a continuous momentum $\mathbf{k}$ along the azimuthal direction, as shown in figure 1(a), satisfying $k_x^2 + k_y^2 = m^2\kappa^2/\hbar^2$. With considering the condensate with SO and ZM coupling, we find that the rotating symmetry of the Hamiltonian is broken, and the single-particle energy has only one minimum at $\left(\kappa\frac{m}{\hbar}, 0\right)$, as shown in figure 1(b). Obviously, it is the ZM coupling that changes the single-particle ground state from an infinitely degenerate state into a unique state and pin the direction of PW in the x direction. When increasing the strength of ZM coupling, this ground state becomes more and

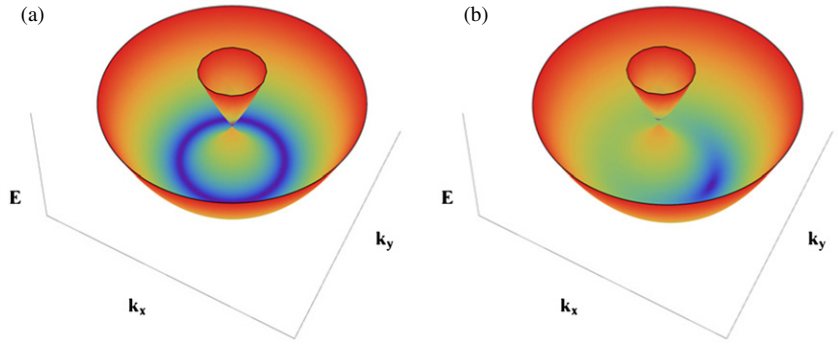

Figure 1. Schematic diagram of single-particle energy–momentum dispersion relations for (a) $\lambda = 0$ and (b) $\lambda \neq 0$. When the ZM coupling is present, the single-particle ground state energy has a minimum at $\left(\kappa\frac{m}{\hbar}, 0\right)$, instead of a continuous circle of degenerate states.

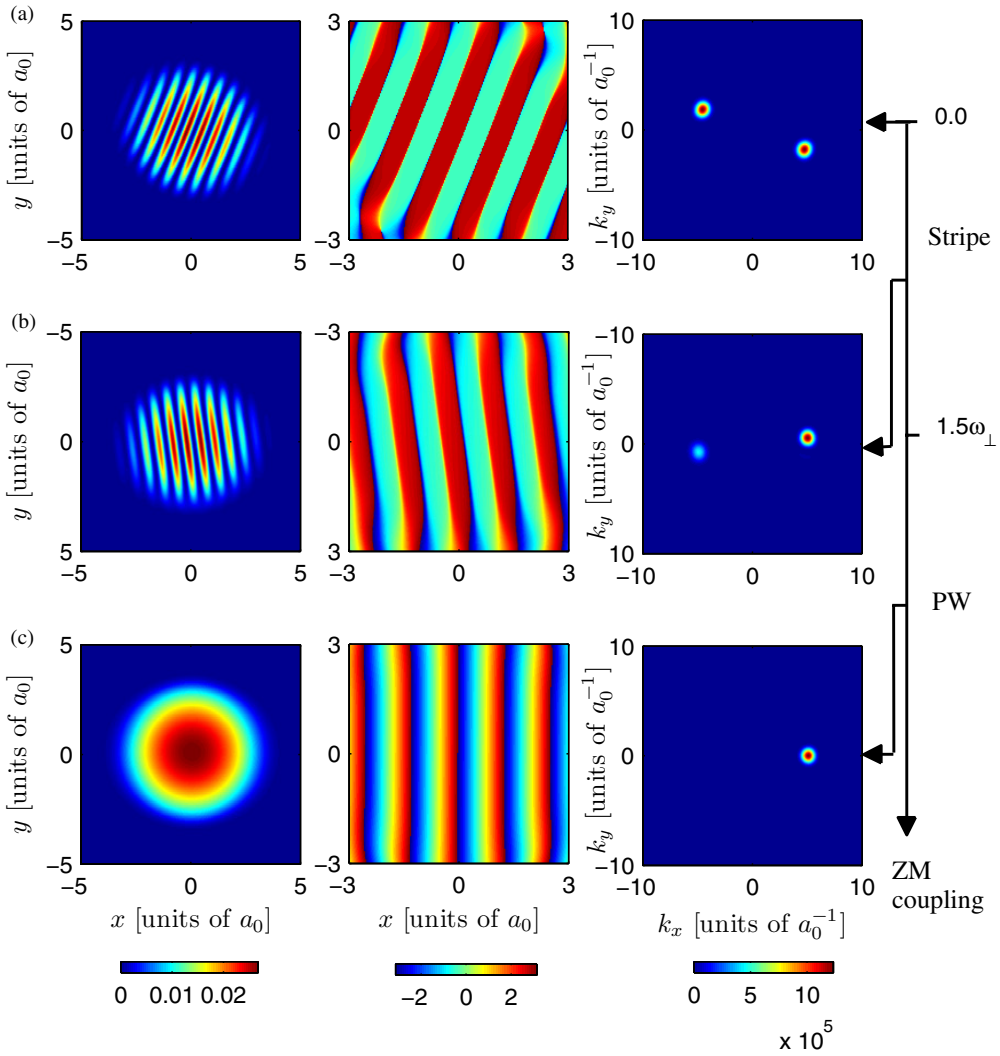

Figure 2. The transition of the condensate from the stripe state to the PW state with the increase of λ. The density profiles of ψ_1 (left), the corresponding phases (middle), and the momentum distributions (right) for (a) $\lambda = 0$, (b) $\lambda = 0.4\omega_\perp$ and (c) $\lambda = 2\omega_\perp$. The intra- and inter-component interactions are chosen as $\tilde{g}_{11} = \tilde{g}_{22} = \tilde{g} = 50$, $\tilde{g}_{12} = 175$, and the strength of SO coupling is fixed at $\kappa = 5\sqrt{\hbar\omega_\perp/m}$. The phase transition point between these two phases is $\lambda = 1.5\omega_\perp$ under this group of parameters.

more energetically separated from the other states on the ring $k_x^2 + k_y^2 = m^2\kappa^2/\hbar^2$. In addition, for the case that $\lambda < 0$, which corresponds to the fact that the change of $\lambda \to -\lambda$ is tantamount to $\psi_2 \to -\psi_2$, $x \to -x$ and $y \to -y$, the single-particle energy has also one minimum at $\left(-\kappa\frac{m}{\hbar}, 0\right)$.

3. Mean-field many-body ground state

In this section, we numerically study the mean-field many body ground states of the system. After rescaling the parameters $\tilde{\mathbf{r}} = \mathbf{r}/a_0$, $\tilde{t} = \omega_\perp t$, $\tilde{E}_\pm = E_\pm/\hbar\omega_\perp$, $\tilde{\lambda} = \lambda/\omega_\perp$,

$\tilde{\kappa} = \kappa\sqrt{\frac{m}{\hbar\omega_\perp}}$, $\tilde{k}_x = k_x a_0, \tilde{k}_y = k_y a_0$, and $\tilde{\psi}_j = \psi_j a_0/\sqrt{N}$ respectively, where $a_0 = \sqrt{\hbar/m\omega_\perp}$, then we obtain the two-dimensional dimensionless coupled Gross–Pitaevskii equations:

$$\mathrm{i}\frac{\partial\tilde{\psi}_1}{\partial\tilde{t}} = \left[-\frac{1}{2}\tilde{\nabla}^2 + \tilde{V} + \left(\tilde{g}_{11}|\tilde{\psi}_1|^2 + \tilde{g}_{12}|\tilde{\psi}_2|^2\right)\right]\tilde{\psi}_1 - \tilde{\kappa}\left(\mathrm{i}\partial_{\tilde{x}} + \partial_{\tilde{y}}\right)\tilde{\psi}_2 + \tilde{\lambda}\tilde{\psi}_2, \quad (3a)$$

$$\mathrm{i}\frac{\partial\tilde{\psi}_2}{\partial\tilde{t}} = \left[-\frac{1}{2}\tilde{\nabla}^2 + \tilde{V} + \left(\tilde{g}_{12}|\tilde{\psi}_1|^2 + \tilde{g}_{22}|\tilde{\psi}_2|^2\right)\right]\tilde{\psi}_2 - \tilde{\kappa}\left(\mathrm{i}\partial_{\tilde{x}} - \partial_{\tilde{y}}\right)\tilde{\psi}_1 + \tilde{\lambda}\tilde{\psi}_1, \quad (3b)$$

where the 2D dimensionless effective interaction coefficients are defined as $\tilde{g}_{jk} = 2\sqrt{2\pi\eta}Na_{jk}/a_0$, by approximating the z dependence of the wave function as a single-particle ground state [33]. Furthermore, the wave functions are normalized as $\sum_j \int |\tilde{\psi}_j|^2 \,\mathrm{d}\tilde{x}\,\mathrm{d}\tilde{y} = 1$.

In the following, we will discuss the effect of ZM coupling on the SO coupled BECs with a weak harmonic trap and a strong harmonic trap, respectively. It should be noted that the strength of the trap is relative to the interatomic interactions, that is, the condensate with a strong harmonic trap requires that the harmonic trap energy $\hbar\omega_\perp$ is higher than the characteristic interaction energy $\tilde{g}_{jk}\hbar\omega_\perp$ $\left(\text{i.e.}\tilde{g}_{jk} < 1\right)$, and the condensate with a weak harmonic trap satisfies $\tilde{g}_{jk} \gg 1$.

3.1. The condensate with a weak harmonic trap

We numerically solve equations (3*a*) and (3*b*) using the imaginary time propagation method [34, 35] to obtain the ground state of the condensate. As we know, for the case that the ZM coupling is absent, the condensate with a weak harmonic trap $\left(\tilde{g}_{jk} \gg 1\right)$ presents two phases classified by the competition of the intra- and inter-component interactions [9]: when $g > g_{12}$, the condensate presents the PW phase, and when $g_{12} > g$, the condensate presents the stripe phase. Recently, it was indicated that in addition to these two phases, there exists another phase, namely a spin polarized ZM phase when $g_{12} > g$ [32]. In this section, we will study the effects of ZM coupling on these three phases, respectively. We choose the intra- and inter-component interactions of the condensate as $\tilde{g}_{11} = \tilde{g}_{22} = \tilde{g} = 50$, $\tilde{g}_{12} = 175$, satisfying $\tilde{g}_{12}^2 > \tilde{g}_{11}\tilde{g}_{22}$ and corresponding to two immiscible components. The strength of the SO coupling is chosen as $\kappa = 5\sqrt{\hbar\omega_\perp/m}$. Without ZM coupling, the condensate presents a stripe state, as shown in figure 2(a). It is a superposition of two PW states with opposite momentums. The density of each component has a π/κ periodic modulation in space, and the total density is always a constant.

We define the equilibrium density difference $d = \left|\psi_j\left(\mathbf{k}_R\right)\right|^2 - \left|\psi_j\left(\mathbf{k}_L\right)\right|^2$ with $\psi_j\left(\mathbf{k}_R\right)\left[\psi_j\left(\mathbf{k}_L\right)\right]$ describing the momentum state with $k_x = \kappa\,[-\kappa]$. When the ZM coupling is present, the momentum distribution of particles becomes imbalanced, increased in the $\psi_j\left(\mathbf{k}_R\right)$ $\left[\psi_j\left(\mathbf{k}_L\right)\right]$ state and decreased in the $\psi_j\left(\mathbf{k}_L\right)\left[\psi_j\left(\mathbf{k}_R\right)\right]$ state for $\lambda > 0\,[\lambda < 0]$. The corresponding wave function is a superposition of a standing wave and a PW, resulting that the amplitude of the spin density stripe decreases, as shown in figure 2(b) with $\lambda = 0.4\omega_\perp$.

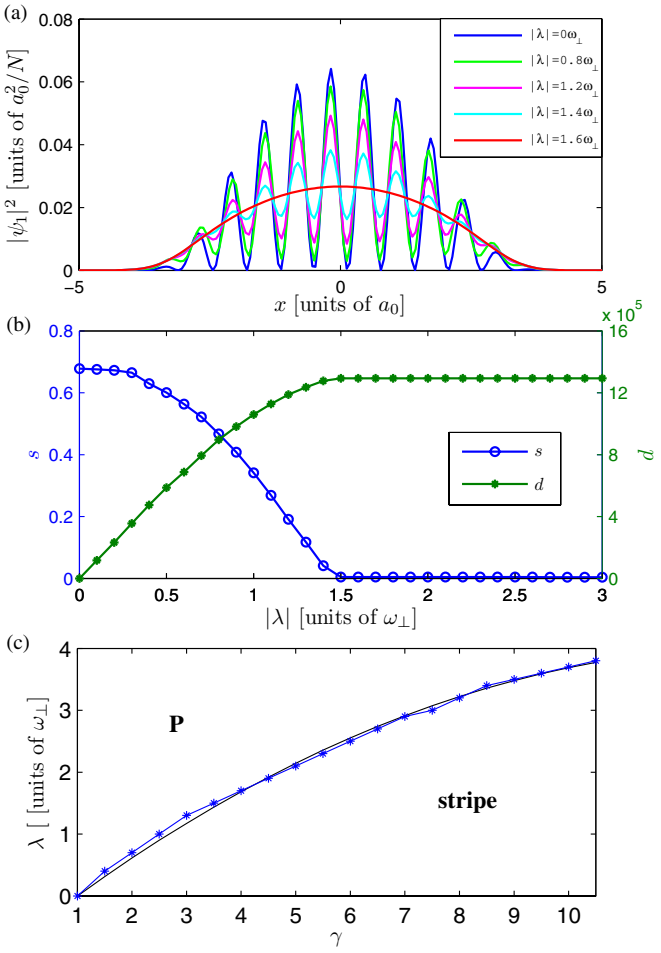

Figure 3. (a) The cross sections of the density $|\psi_1|^2$ with $\gamma = 3.5$ for different λ along the x-axis at $y = 0$, here we rotate the direction of the stripes parallel to the x-axis. (b) The degrees s of phase separation and the differences d between the number of particles distributed at the two k points corresponding to the different ZM coupling $|\lambda|$. For $\lambda > 0$ ($\lambda < 0$), d indicates the particle number on the right (left) minus the one on the left (right). (c) Mean field phase diagram spanned by γ and λ with parameters $\tilde{g} = 50$, $\kappa = 5\sqrt{\hbar\omega_\perp/m}$, where $\gamma = \tilde{g}_{12}/\tilde{g}$. A comparison between the phase boundary obtained by numerical calculation (blue line) and the function $|\lambda| = -0.025\gamma^2 + 0.69\gamma - 0.66$ (black line).

This state can be understood as an intermediate state between the stripe state and the PW state. The effect of ZM coupling on each component is similar, so we only show the density profile of one component in this section. With increasing the coupling strength, the imbalance of particle distribution in k-space is intensified, so the standing wave gradually fades out and the amplitude of the stripe gradually decreases, as shown in figure 3(a). The melting of the spin density stripe can also be understood from that the ZM coupling induces an effective attraction interaction between the two components [27, 36]. Beyond $|\lambda_c| \simeq 1.5\omega_\perp$, all particles distribute at $\left(\kappa\frac{m}{\hbar}, 0\right)$ in k-space and the spin density stripe completely disappears, then the condensate experiences the transition from stripe phase to PW phase, as shown in figure 2. Note that the density distribution changes with $|\lambda|$, and the direction of PW is determined by the sign of λ. In fact, the transitions from stripe phase to PW phase is accompanied by the transition from phase

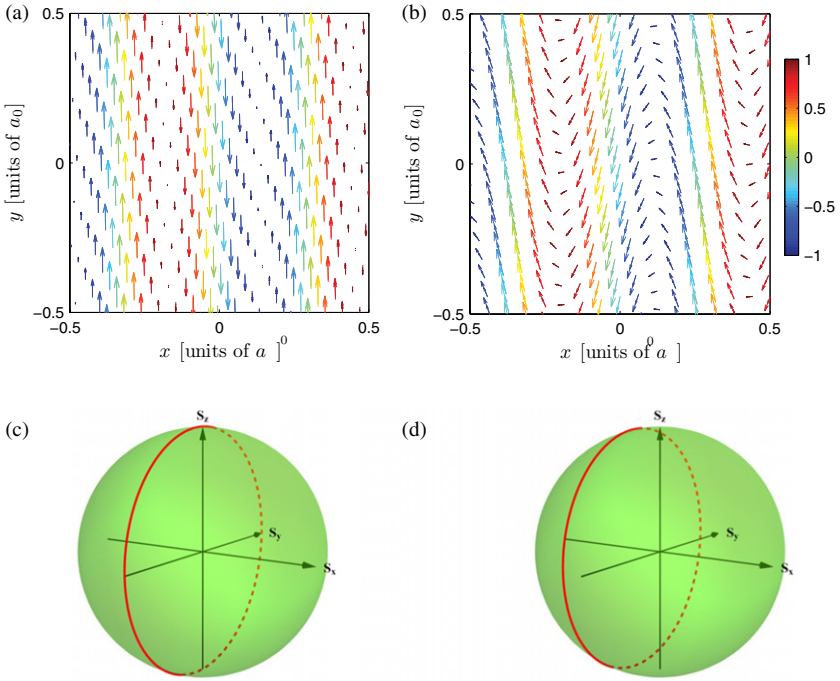

Figure 4. The vectorial plots of the pseudospin S projected onto the x–y plane for (a) $\lambda = 0$, (b) $\lambda = 0.4\omega_\perp$, corresponding to figures 2(a) and (b), respectively. The colours ranging from blue to red describe the values of the axial spin S_z from -1 to 1. (c) and (d) are the projections of pseudospin density vectors of (a) and (b) on the Bloch sphere, respectively.

separation to phase mixture. For a quantitative description of the degree of phase separation, we can use a dimensionless metric

$$s = 1 - \frac{\langle \rho_1 \rho_2 \rangle}{\left(\langle \rho_1^2 \rangle \langle \rho_2^2 \rangle\right)^{1/2}}, \tag{4}$$

where ρ_j $(j = 1, 2)$ is the density of the jth component, and $< \ldots >$ is a spatial average [1]. $s = 0$ denotes complete phase mixture and $s = 1$ denotes complete phase separation.

Figure 3(b) shows the dependence of the degree of phase separation s and the equilibrium density difference d on the strength of ZM coupling $|\lambda|$. We can see that two components are strongly separated at the small λ, and s dramatically decreases with the increase of $|\lambda|$. When $|\lambda| > |\lambda_c| \simeq 1.5\omega_\perp$, $s \simeq 0$ and two components present a mixed state with identical and symmetric density distributions. The equilibrium density difference d increases with the increase of $|\lambda|$, and when $|\lambda| > |\lambda_c| \simeq 1.5\omega_\perp$, all particles distribute in single momentum state so d becomes a constant.

We know that the direction of spin density stripe is chosen spontaneously in the x–y plane without ZM coupling. For later convenience, we define the direction of the stripe perpendicular to the propagation directions of PWs. With increasing the strength of ZM coupling, the direction of the spin density stripe gets closer and closer to the y direction, and eventually is pinned in the y direction, and the direction of the PW in the PW phase is pinned in the x direction, as shown in figure 2. This phenomenon can be understood from the single particle ground state that ZM coupling energetically pins the direction of the PW in x direction.

For simplicity, we define $\gamma = \tilde{g}_{12}/\tilde{g}$, and assume $\tilde{g} = 50$. The strength of SO coupling is fixed at $\kappa = 5\sqrt{\hbar\omega_\perp/m}$. The phase diagram spanned by $|\lambda|$ and γ is presented in figure 3(c). Fitting these numerical phase boundary points, we find that the boundary in figure 3(c) can be presented by a function $|\lambda| = -0.025\gamma^2 + 0.69\gamma - 0.66$, where $\tilde{g} = 50$ is fixed. We can see that the ZM coupling makes the phase boundary between the PW phase and the stripe phase shift, in other words, we can obtain the PW phase even for $\tilde{g}_{12} > \tilde{g}$. So without changing other conditions, the phase transition from stripe phase to PW phase can be realized by increasing the strength of ZM coupling.

We know that the spinor nature of multi-component condensates can be described by introducing pseudospin, and the spinor order parameter of two-component BECs allows us to analyse this system as a pseudospin-1/2 BEC. The pseudospin density vector is defined as $\mathbf{S} = \Psi^\dagger \sigma \Psi / |\Psi|^2$. We decompose it as

$$\begin{cases} S_x = 2\dfrac{|\psi_1||\psi_2|}{|\Psi|^2}\cos(\theta_1 - \theta_2), \\ S_y = -2\dfrac{|\psi_1||\psi_2|}{|\Psi|^2}\sin(\theta_1 - \theta_2), \\ S_z = \left(|\psi_1|^2 - |\psi_2|^2\right)/|\Psi|^2, \end{cases} \tag{5}$$

where θ_j is the phase of the wave function ψ_j and the modulus of the total spin is $|\mathbf{S}| = 1$. Figures 4(a) and (b) show the spin textures of the stripe phase with different λ, where we rotate the direction of spin density stripe in figures 2(a) and (b) to the y-axis. From figure 4(a) we can see that the stripe phase presents a spin spiral state when ZM coupling is absent. ψ_1 corresponds to the up component of the spin-1/2 spinor and ψ_2 corresponds to its down component. At the interfaces of the two components, the spin density vectors flip from up to down forming a train of domain walls in the type of the classical

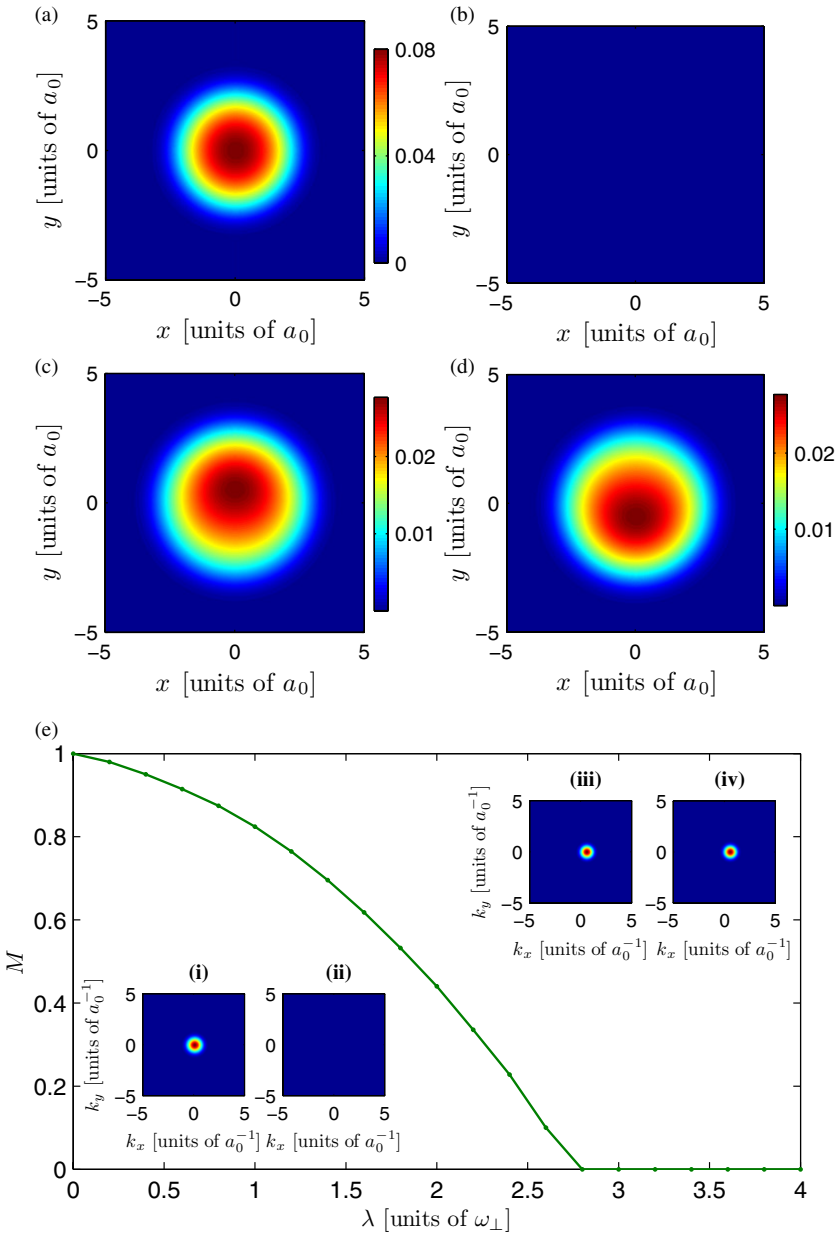

Figure 5. The transition of the condensate from the ZM state to the PW state with the increase of λ. The density profiles of (a) ψ_1, (b) ψ_2 with $\lambda = 0$. Furthermore, the density profiles of (c) ψ_1, (d) ψ_2 with $\lambda = 3\omega_\perp$. (e) The polarization M corresponding to the different ZM coupling, and the insets (i), (ii), (iii) and (iv) present the momentum distributions corresponding to (a), (b), (c) and (d). The intra- and inter-component interactions are chosen as $\tilde{g}_{11} = \tilde{g}_{22} = \tilde{g} = 50$, $\tilde{g}_{12} = 175$, and the strength of SO coupling is fixed at $\kappa = 0.5\sqrt{\hbar\omega_\perp/m}$.

Bloch wall. The spin orientation in the x–y plane depends on the relative phase, and can be represented by an azimuthal angle $\alpha = \arctan(S_y/S_x) = \theta_2 - \theta_1$. For each component of the stripe phase, the periodic density modulation is assumed along the x direction, so the curvature of the density in the y direction can be neglected in the Thomas–Fermi approximation. In addition, from the second plot in figure 2(a) we can see that the phase changes alternately between two constants in the central region, so the curvature of the phase is 0. In the edge region, the non zero curvature of the phase is caused by numerical error. We ignore the non zero curvature of the phase, because the particle distribution is almost zero in the edge region, and we only care about the region of the centralized particles' distribution. So with replacing $\psi_j = \sqrt{\rho_j}\, e^{i\theta_j}$, we obtain $\partial_y\sqrt{\rho_j} = 0$ and $\partial_x\theta_j = \partial_y\theta_j = 0$. Substituting them into the last two terms of equation (1*a*), we obtain $E = \int d\mathbf{r}\left\{2\kappa\sqrt{\rho_2}\partial_x\sqrt{\rho_1}\sin(\theta_1 - \theta_2)\right\}$. Minimizing the energy, we obtain the azimuthal angle $\alpha = \frac{\pi}{2}$ for $\partial_x\sqrt{\rho_1} > 0$, and $\alpha = -\frac{\pi}{2}$ for $\partial_x\sqrt{\rho_1} < 0$, thus the spin density vector forms the spin flipping as shown in figure 4(a).

When ZM coupling is present, the spin density vectors are tilted towards the x direction at some angle, and the texture becomes a periodic wavy spin spiral, as shown in figure 4(b). The curvature of the density in the y direction can also be neglected. When the momentum distribution at the two points becomes seriously imbalanced, the wave function can

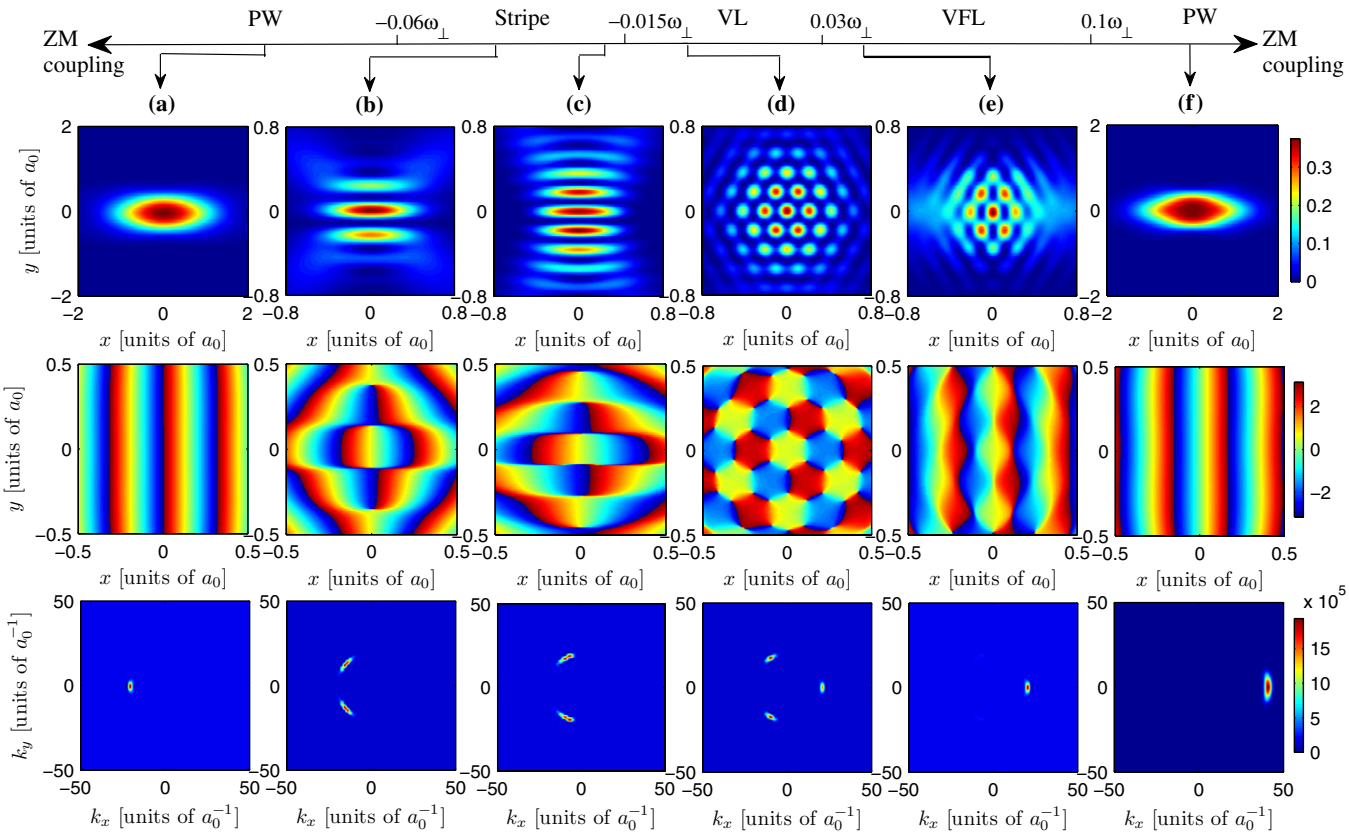

Figure 6. The density profiles (first line), the phase profiles (second line) and the momentum distributions (third line) of the ground state with different λ. (a) $\lambda = -0.1\omega_\perp$, (b) $\lambda = -0.04\omega_\perp$, (c) $\lambda = -0.02\omega_\perp$, (d) $\lambda = 0$, (e) $\lambda = 0.04\omega_\perp$ and (f) $\lambda = 0.2\omega_\perp$. Increasing $|\lambda|$ from the initial VL state, (d) → (e) → (f), the condensate experiences the transitions from VL state to VFL state and finally to PW state, with the critical values $\lambda = 0.03\omega_\perp$ and $\lambda = 0.1\omega_\perp$. (d) → (c) → (b) → (a), the condensate experiences the transitions from the VL state to the stripe state and finally to the PW state with the critical values $\lambda = -0.015\omega_\perp$ and $\lambda = -0.06\omega_\perp$. The intra- and inter-component interactions are chosen as $\tilde{g}_{11} = \tilde{g}_{22} = \tilde{g} = 0.2$, $\tilde{g}_{12} = 0.3$, and the strength of SO coupling is fixed at $\kappa = 20\sqrt{\hbar\omega_\perp/m}$.

be approximated as a PW, so the curvature of the phase in x direction can be approximated as the SO coupling strength κ. So we obtain $\partial_y\sqrt{\rho_j} = 0$, $\partial_x\theta_j \simeq \kappa$ and $\partial_y\theta_j = 0$. Substituting them into the last two terms of equation (1*a*), and using the auxiliary angle formula of the trigonometric function, we obtain $E = \int \mathrm{d}\mathbf{r}\,\{A\sin(\theta_1 - \theta_2 + \beta)\}$, where $A = \sqrt{4\kappa^2\rho_2\left(\partial_x\sqrt{\rho_1}\right)^2 + 4\left(\kappa^2+\lambda\right)^2\rho_1\rho_2}$, and $\beta = n\pi + \arctan\frac{2(\kappa^2+\lambda)\rho_1}{\kappa\partial_x\rho_1}$, $(n = 0, \pm1, \pm2, \ldots)$ is an auxiliary angle. We choose $\theta_1 - \theta_2 + \beta = -\frac{\pi}{2}$ to minimize the energy, so the azimuthal angle becomes $\alpha = \frac{\pi}{2} + \beta$, where $\beta = \arctan\frac{2(\kappa^2+\lambda)\rho_1}{\kappa\partial_x\rho_1}$ for $\partial_x\rho_1 > 0$; and $\beta = -\pi + \arctan\frac{2(\kappa^2+\lambda)\rho_1}{\kappa\partial_x\rho_1}$ for $\partial_x\rho_1 < 0$. Note that $\sin\beta = 2\sqrt{\rho_1\rho_2}\left(\kappa^2+\lambda\right)/A$ is always positive, soα is limited in range $\left(-\pi, -\frac{\pi}{2}\right)$ or $\left(\frac{\pi}{2}, \pi\right)$ and varies periodically, as shown in figure 4(b). With the increase of λ, the spin density vectors become more tilted and topple completely in the end, accompanied by the phase transition from stripe phase to PW phase. At this point, $\partial_x\rho_1 = 0$, $\beta = \frac{\pi}{2}$ and $\alpha = \pi$, all spin density vectors are aligned along the opposite direction of the x-axis. That is because that the ZM frequency may be regarded as a transverse (pseudo)magnetic field that aligns the spin along the x-axis. For the case that $\lambda < 0$, the spin density vectors tilt in the opposite directions.

The projections of the spin density vectors in figures 4(a) and (b) onto the surface of a Bloch sphere are shown in figures 4(c) and (d), respectively. We can see that when $\lambda = 0$, the spin density vectors just cover the sphere on a meridian in the y–z plane. With increasing λ, they cover the sphere on a circle which is parallel to the y–z plane with a smaller radius. As λ increases further, the circle shrinks gradually to a point at the surface of the Bloch sphere.

Keeping the intra- and inter-component interactions in figure 2 unchanged, i.e. $\tilde{g}_{11} = \tilde{g}_{22} = \tilde{g} = 50$, $\tilde{g}_{12} = 175$, and choosing quite a weak SO-coupling strength, e.g. $\kappa = 0.5\sqrt{\hbar\omega_\perp/m}$, we obtain a spin polarized ZM phase when the ZM coupling is absent. The condensate is fully polarized and occupies ZM, i.e. the polarization $M = \int\left[|\psi_1|^2 - |\psi_2|^2\right]\mathrm{d}\mathbf{r} / \int\left[|\psi_1|^2 + |\psi_2|^2\right]\mathrm{d}\mathbf{r} = 1$ and $\mathbf{k} = \mathbf{0}$ as shown in figures 5(a), (b) and (e). The presence of ZM coupling induces an effective attraction between the two components, so half of the atoms shift from the ψ_1 state to the ψ_2 state and the condensate becomes an unpolarized one. When $|\lambda| > |\lambda_c| \simeq 2.8\omega_\perp$, the condensate presents a mixed state and the two components have the same particle number, as shown in figures 5(c) and (d) with $\lambda = 3\omega_\perp$. From the insets (iii) and (iv) in figure 5(e) we can see that the momentum distributions of two components are no longer equal to 0, but

$\left(\kappa\frac{m}{\hbar}, 0\right)$. The condensate experiences the transition from ZM phase to PW phase.

3.2. The condensate with a strong harmonic trap

We know that the SO coupled BECs will emerge as VL phases [12, 17–19] spontaneously in the strong trap region $\left(\tilde{g}_{jk} < 1\right)$. Furthermore, Xu *et al* point out that the momentum distributions of these VL phases may be three points, four points or six points, around the ring of radius $\kappa\frac{m}{\hbar}$ [18]. A systematic understanding about which phase will emerge is still elusive as a lot of previous results are obtained by solving the coupled Gross–Pitaevskii equations numerically. We take the parameters from [17] $\tilde{g}_{11} = \tilde{g}_{22} = \tilde{g} = 0.2$, $\tilde{g}_{12} = 0.3$, and $\kappa = 20\sqrt{\hbar\omega_\perp/m}$. After numerical calculation we found that the vortex lattice phase with three-point momentum distribution has lower energy. Taking this phase as an example, we will study the effect of ZM coupling on the VL phases induced by SO coupling instead of rotation in the following.

When the ZM coupling is absent, the condensate with a strong SO coupling presents a VA lattice in each component, as shown in figure 6(d). Half of these vortices in one component are filled with the density peaks of the other component, forming HQV, and the sign of HQV is determined by the vortex sign and the component in which the vortex resides. In addition, the other half of the vortices in both components are coincident with opposite sign. So the total density profile is a VL rather than a smooth bell, and the relative phases in these singularities have 4π difference. The formation of this vortex lattice structure can be understood as a superposition of three k points in momentum space as shown in figure 6(d). It should be noted that the positions of these three points on the ring of radius $\kappa\frac{m}{\hbar}$ is not unique, since the symmetry is broken spontaneously, i.e. $\varphi_k = \bar{\varphi} + (l-1)\frac{2\pi}{3}$, $(l = 1, 2, 3)$, here $\varphi_k = \arg(k_x + \mathrm{i}k_y)$ and $\bar{\varphi}$ being arbitrary. In this section, we choose $\bar{\varphi} = 0$, then the momentum distribution is determined, as shown in figure 6(d).

From the effect of λ on the condensate with a weak harmonic trap, we know that the sign of λ would not change the particle density distribution, but only change the direction of the phase gradient. That is because the two k points of particle distribution in k-space are centre symmetric. The situation for the condensate with a strong harmonic trap is complicated, because the three k points of the momentum distribution constitute a triangular structure, destroying the symmetry. So there will be different profiles of the ground states for different signs of λ. We first consider the situations of $\lambda < 0$. The density profiles, the phases and the momentum distributions are shown in figures 6(c), (b) and (a). With the increase of $|\lambda|$, the particle distribution in k-space becomes imbalanced, increased at the left two points and decreased at the right point. When $|\lambda| \geqslant 0.015\omega_\perp$, only two are left from these three k points, as shown in figure 6(c) with $\lambda = -0.02\omega_\perp$. We can see that these two k points have the same x-value $k_x = -\frac{\kappa m}{2\hbar}$ and the opposite y-value $k_y = \pm\frac{\sqrt{3}\kappa m}{2\hbar}$. It means that all particles are condensated into a state with the same momentum in x direction and opposite momentum in y direction, then a stripe state with a modulation period of π/k_y is obtained.

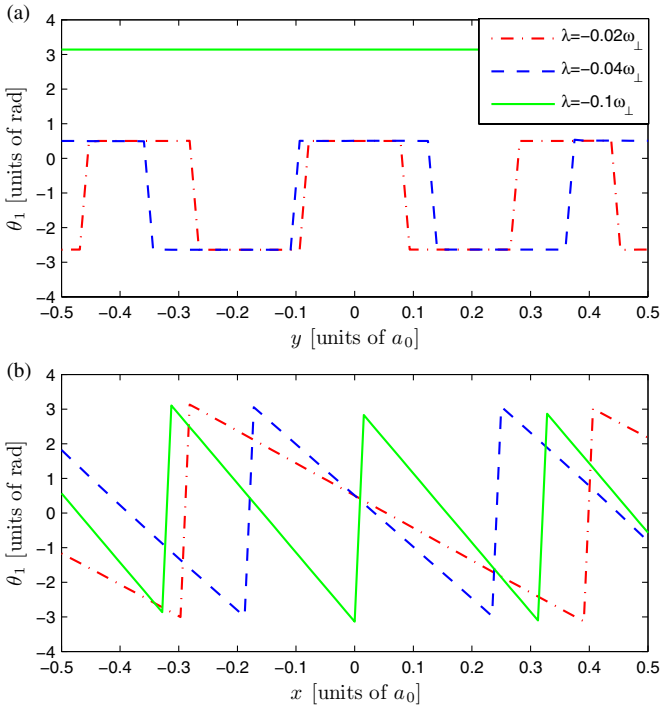

Figure 7. Section views of the phase θ_1 (a) along the y-axis and (b) along the x-axis with $\lambda = -0.02\omega_\perp$ (red dashed–dotted line), $\lambda = -0.04\omega_\perp$ (blue dashed line) and $\lambda = -0.1\omega_\perp$ (green solid line).

This stripe state is different from the one researched by Wang *et al*, because their stripe direction is spontaneously chosen in the x–y plane, but our stripe direction is fixed in x direction. More importantly, their phase of the stripe state presents a standing wave perpendicular to the stripe direction, but our phase presents not only a standing wave perpendicular to the stripe direction, but also a PW along the stripe direction, as shown in figure 7, meaning nonzero superfluid velocity along the stripe. As $|\lambda|$ increases, the two k points gradually close to each other along the circle $k_x^2 + k_y^2 = m^2\kappa^2/\hbar^2$. The wave number of the PW in x direction increases, and the one of the standing wave in y direction decreases. So the modulation period of the stripe increases and the one of the PW decreases, as shown in figure 6(b) with $\lambda = -0.04\omega_\perp$ and figure 7. When $|\lambda| \geqslant 0.06\omega_\perp$, the ZM coupling drives the condensate from a stripe state to a PW state, and all particles distribute at $\left(-\kappa\frac{m}{\hbar}, 0\right)$ in k-space, as shown in figure 6(a) with $\lambda = -0.1\omega_\perp$, agreeing with the effect of ZM coupling on the single-particle ground state.

Next we consider the situations for $\lambda > 0$. The density profiles, the phases and the momentum distributions are shown in figures 6(e) and (f). In order to study the effect of λ on VA pairs in more detail, we also plot the cross sections of density profiles of the ψ_1 component along the y direction at $x = 0$ with different λ in figure 8. We can see that the density barriers between the VA pairs are reduced and the VA pairs are close to each other with the increase of λ. Meanwhile, the coincident vortices located in different components are deviated from each other. The momentum distribution at three k points becomes imbalanced, increased at the k point on the right and decreased at the other two points on the left.

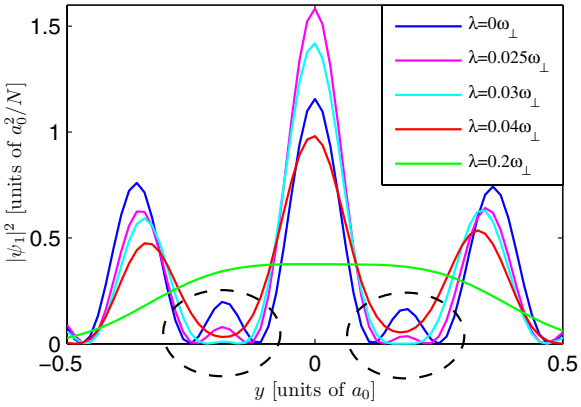

Figure 8. The cross sections of the density $|\psi_1|^2$ with $\tilde{g}_{11} = \tilde{g}_{22} = \tilde{g} = 0.2$, $\tilde{g}_{12} = 0.3$, and $\kappa = 20\sqrt{\hbar\omega_\perp/m}$, for different λ along the x-axis at $y = 0$. The black dotted circles indicate the region of VA pairs. The vortex and antivortex are close to and annihilate each other with the increase of λ.

When $\lambda > 0.03\omega_\perp$, the density barriers disappeared, so the vortex and the antivortex slip into the same hole and eventually annihilate, as shown in figure 6(e) with $\lambda = 0.04\omega_\perp$. From the density profile of each component, we can see that the holes still exist, but the singularities in the phase diagram vanish, which means no vortex. So we name this new structure a VFL. This state can be understood as an intermediate state between the VL state and the PW state. At this point, the particles still distribute at three points in k-space, but their distribution on the left is too few to be observed. As λ increases further, $\lambda \geqslant 0.1\omega_\perp$, the VFL disappears and the density profile becomes smooth, meanwhile, all particles distribute at $\left(\kappa\frac{m}{\hbar}, 0\right)$ in k-space and the phase becomes a PW, as shown in figure 6(f) with $\lambda = 0.2\omega_\perp$. Noting that if the momentum distribution of the initial vortex state has one peak on the left and two peaks on the right, i.e. $\bar{\varphi} = \frac{\pi}{3}$, all the scenarios presented in figure 6 would be inversed horizontally.

The pseudospin texture of the VL phase is shown in figure 9(a) with $\lambda = 0$. This texture is the same as the ones in the [17] if we exchange ψ_1 and ψ_2, and exchange S_x and S_y. Figure 9(b) is an amplified local part of (a), and we classify three kinds of textures labelled (i), (ii) and (iii), which correspond to + HQV, −HQV and spin-2 texture, respectively. The spin-2 textures are located at the position of the coincident vortices with opposite sign that reside in different components, with winding number −2. The projection of these vectors onto the surface of a Bloch sphere is shown in figure 10(a). ±HQV cover the Bloch sphere hemisphere once respectively, and spin-2 texture wraps the Bloch sphere twice.

When the ZM coupling is present, the arrangement of ±HQV is changed, due to the distance of VA pairs decreasing, as shown in figure 9(c) with $\lambda = 0.03\omega_\perp$. From figures 9(c) and (d) we can see that the spin density vectors are squeezed transversely and the spin textures are deformed compared to the ones shown in figure 9(a). These spin density vectors cover the Bloch sphere with a partial loss, i.e. they cover an incomplete sphere as shown in figure 10(b) with $\lambda = 0.02\omega_\perp$ and (c) with $\lambda = 0.03\omega_\perp$, because of the effect of ZM coupling. With the increase of λ, the transition from VL state to VFL

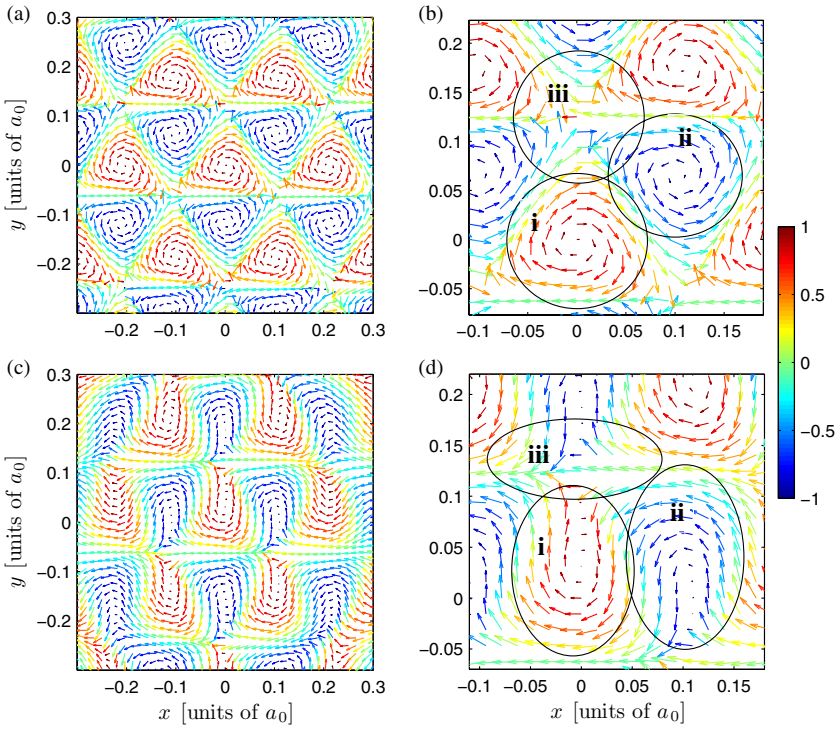

Figure 9. (a) The vectorial plots of the pseudospin S projected onto the x–y plane corresponding to the ground state in figure 5(a) with $\tilde{g}_{11} = \tilde{g}_{22} = \tilde{g} = 0.2$, $\tilde{g}_{12} = 0.3$, $\kappa = 20\sqrt{\hbar\omega_\perp/m}$, and $\lambda = 0$. Values of S_z are represented by linear levels from blue to red (−1 to 1). (b) An amplified local part of (a). Here the regions of (i), (ii) and (iii) indicate the +HQV, −HQV and spin-2 texture, respectively. (c) The vectorial plots of the pseudospin S projected onto the x–y plane with $\lambda = 0.03\omega_\perp$. (d) An amplified local part of (c). Corresponding to (a) and (b), the spin density vectors pointing to the x direction are suppressed and the spin texture is deformed with the effect of ZM coupling.

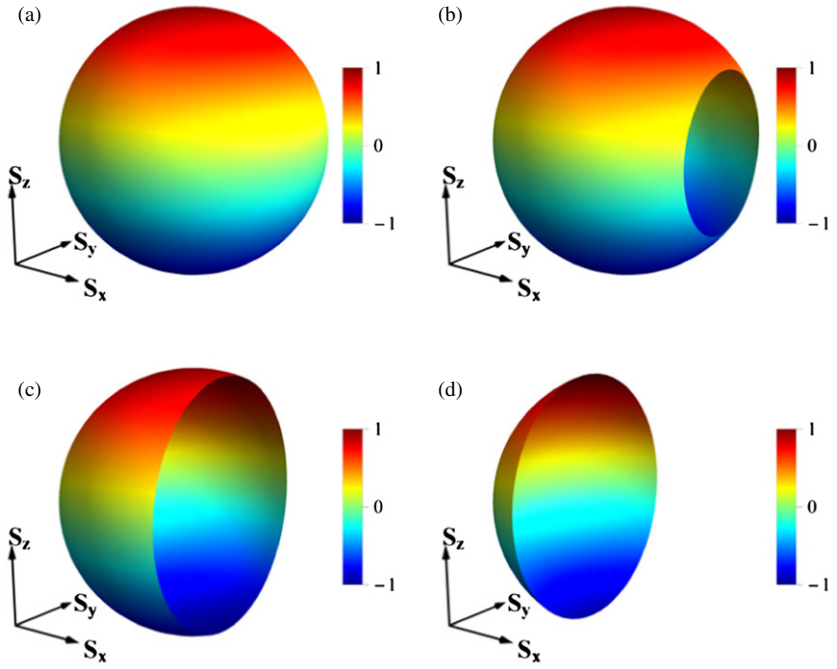

Figure 10. The projections of pseudospin density vectors on the Bloch sphere for (a) $\lambda = 0$, (b) $\lambda = 0.02\omega_\perp$, (c) $\lambda = 0.03\omega_\perp$ and (d) $\lambda = 0.04\omega_\perp$, indicating the suppression of the ZM coupling on the spin orientation. The colour scaling from blue to red means the values of S_z from -1 to 1.

state is accompanied by a change of the covered Bloch sphere from more than half of the sphere to less than half of the sphere, as shown in figure 10(d) with $\lambda = 0.04\omega_\perp$. As $\lambda \geqslant 0.1\omega_\perp$, the condensate presents the PW state and the corresponding spin density vectors eventually narrow down to a point at the surface of the Bloch sphere.

4. Experimental proposal

In real experiments, we can select two internal spin states within the ^{39}K BEC system $|F = 1, m_f = 0\rangle$ and $|F = 1, m_f = 1\rangle$ labelled pseudospin up and pseudospin down, respectively, in the weak trap region, as ^{39}K has proven to be a good candidate for realizing Feshbach resonance in experiments [37, 38]. The condensate contains about 10^4 atoms. The trapping frequencies of the potential can be chosen as $\{\omega_\perp, \omega_z\} = 2\pi \times \{4.5, 22.5\}$ Hz, and the scattering lengths are adjusted as $a_{11} = a_{22} \approx 58a_B$, $a_{12} \approx 204a_B$ (a_B is the Bohr radius) which are consistent with our previous dimensionless interaction parameters $\tilde{g}_{11} = \tilde{g}_{22} = 50$, $\tilde{g}_{12} = 175$. When the SO coupling strength is chosen as $\kappa = 5\sqrt{\hbar\omega_\perp/m}$, with increasing the ZM coupling strength from $\lambda = 0$ to $1.2\omega_\perp$, and finally to $2\omega_\perp$, we can observe the condensate transitions from stripe phase to PW phase by monitoring the density profiles and phases of the condensate. When the SO coupling strength is chosen as $\kappa = 0.5\sqrt{\hbar\omega_\perp/m}$, we can observe the transitions from ZM phase to PW phase with increasing the ZM coupling strength from $\lambda = 0$ to $3\omega_\perp$. In the strong trap region, the trapping frequencies can also be chosen as $\{\omega_\perp, \omega_z\} = 2\pi \times \{4.5, 22.5\}$ Hz, but the scattering lengths are adjusted as $a_{11} = a_{22} \approx 0.26a_B$, $a_{12} \approx 0.38a_B$. Fixing the SO coupling strength $\kappa = 20\sqrt{\hbar\omega_\perp/m}$ and adjusting the strength of ZM coupling from $\lambda = 0$ to $0.04\omega_\perp$, and then to $0.2\omega_\perp$, we can observe the condensate transitions from a VL state to a VFL state and then to a PW state. For the case of $\lambda < 0$, adjusting the strength of ZM coupling from $\lambda = 0$ to $-0.02\omega_\perp$, and then to $-0.1\omega_\perp$, we can observe the condensate transitions from a VL state to a stripe state and finally to PW state.

5. Conclusion

In summary, we have studied the transitions of ground states induced by ZM coupling in pseudospin-1/2 Rashba SO coupled BECs confined in a harmonic potential. We have calculated the single-particle ground state without considering the external trap and found that the presence of the ZM coupling changes the ground state from an infinitely degenerate state into a nondegenerate state. We have also numerically studied the mean-field many-body ground states of the condensates. For the SO coupled condensate with a weak harmonic trap, the condensate exhibits a PW state, a stripe state or a ZM state. For the stripe state, the amplitude of the stripe decreases with the increase of ZM coupling, and this stripe state is different from the ones mentioned in previous works, because of the imbalanced particle distribution in k-space. When the strength of ZM coupling exceeds a critical value, the stripes disappear completely and the condensate experiences the transition from the stripe state to the PW state. The phase boundary between the PW phase and the stripe phase is shifted. Moreover, the transition from the ZM state to the PW state can also be realized by ZM coupling. So performing a ZM coupling on the SO-coupled BECs is another method to realize the transition from stripe phase or ZM phase

to PW phase, besides adjusting the interatomic interactions realized by Feshbach resonance.

We have also studied the ground state of a condensate under a strong harmonic trap with or without ZM coupling. When the ZM coupling is absent, the arrangement of the VA pairs in both components leads to three kinds of spin textures: ±HQV and spin-2 texture. When the ZM coupling is present, we have discussed the impacts of the sign of the effective Rabi frequency on the structures of the ground states. When $\lambda > 0$, the condensate experiences the transitions from the VL state to the VFL state and then to the PW state. Furthermore, when $\lambda < 0$, the condensate experiences the transitions from the VL state to the stripe state and then to the PW state. The direction of the PW is opposite for the different sign of λ, and the stripe state mentioned here is different from the ones mentioned in previous works, because of its nonzero superfluid velocity along the stripe. We have developed a new way to manipulate the SO-coupled BEC system. This work will make it possible to simulate more interesting problems in more general quantum many-body systems, such as the half-vortex state for quantum information storage and the explorations of new phases of condensed matter.

Acknowledgments

This work was supported by the National Natural Science Foundation of China (10972125), Specialized Research Fund for the Doctoral Program of Higher Education of China (20111401110004), Natural Science Foundation of Shanxi Province (2010011001-2) and Project Supported by Shanxi Scholarship Council of China.

References

[1] Lin Y-J, Jiménez-García K and Spielman I B 2011 *Nature* **471** 83
[2] Kato Y K, Myers R C, Gossard A C and Awschalom D D 2004 *Science* **306** 1910
[3] König M, Wiedmann S, Brüne C, Roth A, Buhmann H, Molenkamp L W, Qi X-L and Zhang S-C 2007 *Science* **318** 766
[4] Žutić I, Fabian J and Das Sarma S 2004 *Rev. Mod. Phys.* **76** 323
[5] Sinova J, Culcer D, Niu Q, Sinitsyn N A, Jungwirth T and MacDonald A H 2004 *Phys. Rev. Lett.* **92** 126603
[6] Bernevig B A, Hughes T L and Zhang S-C 2006 *Science* **314** 1757
[7] Hasan M Z and Kane C L 2010 *Rev. Mod. Phys.* **82** 3045
[8] Qi X-L and Zhang S-C 2011 *Phys. Today* **63** 33
[9] Wang C, Gao C, Jian C M and Zhai H 2010 *Phys. Rev. Lett.* **105** 160403
Zhai H 2012 *Int. J. Mod. Phys.* B **26** 1230001
[10] Jian C M and Zhai H 2011 *Phys. Rev.* B **84** 060508
[11] Ho T-L and Zhang S 2011 *Phys. Rev. Lett.* **107** 150403
[12] Sinha S, Nath R and Santos L 2011 *Phys. Rev. Lett.* **107** 270401
[13] Kawakami T, Mizushima T and Machida K 2011 *Phys. Rev.* A **84** 011607
[14] Xu Z F, Lü R and You L 2011 *Phys. Rev.* A **83** 053602
[15] Zhang Y, Mao L and Zhang C 2012 *Phys. Rev. Lett.* **108** 035302
[16] Su S W, Liu I K, Tsai Y C, Liu W M and Gou S C 2012 *Phys. Rev.* A **86** 023601
[17] Hu H, Ramachandhran B, Pu H and Liu X J 2012 *Phys. Rev. Lett.* **108** 010402
[18] Xu Z F, Kawaguchi Y, You L and Ueda M 2012 *Phys. Rev.* A **86** 033628
[19] Ramachandhran B, Opanchuk B, Liu X J, Pu H, Drummond P D and Hu H 2012 *Phys. Rev.* A **85** 023606
[20] Ozawa T and Baym G 2012 *Phys. Rev. Lett.* **109** 025301
[21] Zhou X-F, Zhou J and Wu C 2011 *Phys. Rev.* A **84** 063624
[22] Xu X Q and Han J H 2011 *Phys. Rev. Lett.* **107** 200401
[23] Radić J, Sedrakyan T A, Spielman I B and Galitski V 2011 *Phys. Rev.* A **84** 063604
[24] Hall D S, Matthews M R, Wieman C E and Cornell E A 1998 *Phys. Rev. Lett.* **81** 1543
[25] Matthews M R, Anderson B P, Haljan P C, Hall D S, Holland M J, Williams J E, Wieman C E and Cornell E A 1999 *Phys. Rev. Lett.* **83** 3358
[26] Merhasin M I, Malomed B A and Driben R 2005 *J. Phys. B: At. Mol. Opt. Phys.* **38** 877
[27] Kasamatsu K, Tsubota M and Ueda M 2004 *Phys. Rev. Lett.* **93** 250406
[28] Shin Y, Jo G-B, Saba M, Pasquini T A, Ketterle W and Pritchard D E 2005 *Phys. Rev. Lett.* **95** 170402
[29] Chang M S, Qin Q, Zhang W, You L and Chapman M S 2005 *Nature Phys.* **1** 111
[30] Bao W and Cai Y 2011 *East Asian J. Appl. Math.* **1** 49–81
[31] Jiménez-García K, LeBlanc L J, Williams R A, Beeler M C, Perry A R and Spielman I B 2012 *Phys. Rev. Lett.* **108** 225303
[32] Yu Z-Q 2013 *Phys. Rev.* A **87** 051606
[33] Kasamatsu K, Tsubota M and Ueda M 2003 *Phys. Rev.* A **67** 033610
[34] Dalfovo F and Stringari S 1996 *Phys. Rev.* A **53** 2477
Chiofalo M L, Succi S and Tosi M P 2000 *Phys. Rev.* E **62** 7438
[35] Bao W, Chern I-L and Lim F Y 2006 *J. Comput. Phys.* **219** 836
[36] García-Ripoll J J, Pérez-García V M and Sols F 2002 *Phys. Rev.* A **66** 021602
Sols F 2002 *Phys. Rev.* A **66** 021602
[37] Roati G, Zaccanti M, D'Errico C, Catani J, Modugno M, Simoni A, Inguscio M and Modugno G 2007 *Phys. Rev. Lett.* **99** 010403
[38] Smith R P, Campbell R L D, Tammuz N and Hadzibabic Z 2011 *Phys. Rev. Lett.* **106** 250403